

Emergent curved space and gravitational lensing in quantum materials

Yugo Onishi,^{1,*} Nisarga Paul,^{1,†} and Liang Fu¹

¹*Department of Physics, Massachusetts Institute of Technology, Cambridge, MA 02139, USA*

(Dated: October 7, 2025)

We show that an effective gravitational field naturally emerges in quantum materials with long-wavelength spin (or pseudospin) textures. When the itinerant electrons' spin strongly couples to the background spin texture, it effectively behaves as a spinless particle in a curved space, with the curvature arising from quantum corrections to the electron's spin orientation. The emergent curved space gives rise to the electron lensing effect, an analog of the gravitational lensing. The lensing effect can appear in systems without (emergent) magnetic fields, such as those with coplanar spin textures. Our work shows that novel "gravitational" phenomena generically appear in quantum systems due to nonadiabaticity, opening new research directions in quantum physics.

Introduction. — A fascinating aspect of quantum physics is the emergence of new particles and fields in systems of electrons. One example is the emergent gauge field. In a system of itinerant electrons strongly coupled to localized spins, a gauge field naturally emerges from the coupling between the electrons and the localized spins in the strong coupling limit, realizing an effective magnetic field acting on the itinerant electrons [1–6]. This effective magnetic field further gives rise to the Hall effect without external magnetic fields [7–12] and flat Chern bands that mimic Landau levels [13].

In this work, we show that an effective gravitational field naturally emerges in quantum materials with long-wavelength spin (or pseudospin) textures by considering the correction from the strong coupling limit. Specifically, when electrons are coupled to localized spins, they are effectively described as spinless particles in a curved space, as depicted in Fig. 1. The curved space gives rise to an electron lensing effect, an analog of gravitational lensing [14]. This effect becomes more significant for fast electrons than slow electrons, in contrast to the scattering due to the effects of a scalar potential.

General theory. — We consider itinerant electrons coupled with localized spins in general d -dimensions:

$$H = \frac{(\mathbf{p} - e\mathbf{A})^2}{2m} - J\mathbf{S}(\mathbf{x}) \cdot \boldsymbol{\sigma}, \quad (1)$$

where $e (< 0)$, m , \mathbf{p} , $\boldsymbol{\sigma}$ are the charge, mass, momentum, and spin of the itinerant electrons, \mathbf{A} is the vector potential describing the external magnetic field, and $\mathbf{S}(\mathbf{x})$ is the localized spin at position \mathbf{x} , with normalization $|\mathbf{S}| = 1$. J is the coupling constant between the electrons and the localized spins. When J is the largest energy scale, the spin of the itinerant electrons is effectively frozen so that their spins almost always align with the local spin $\mathbf{S}(\mathbf{x})$ and can be treated adiabatically.

When J is finite, high-order terms become important. Our focus is on the low-energy effective theory up to $\mathcal{O}(J^{-1})$. To derive the effective theory, we apply the unitary transformation to rotate electron's spin to align with the local axis: $U^\dagger(\mathbf{x})(\mathbf{S}(\mathbf{x}) \cdot \boldsymbol{\sigma})U(\mathbf{x}) = \sigma_z$. The new

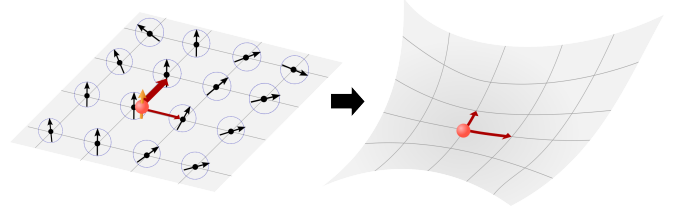


FIG. 1. Schematic illustration of emergent curved space: a spinful electron in a slowly varying spin texture is equivalent to a spinless electron in a curved space, whose metric encodes the "stretching" of real-space distances by the spin texture.

Hamiltonian H' in the basis defined by $U(\mathbf{x})$ is [15, 16]

$$H' = U^\dagger(\mathbf{x})HU(\mathbf{x}) = \frac{(\mathbf{p} - e\mathbf{A} - \hbar\mathbf{a})^2}{2m} - J\sigma_z. \quad (2)$$

Here, $\mathbf{a} = U^\dagger i\nabla U$ is the $U(2)$ gauge field associated with $U(\mathbf{x})$. From Hamiltonian (2), we show that the effective description reduces to spinless electrons in curved space.

Before presenting the general theory, we consider a simple example of a spiral spin texture with wavevector \mathbf{q} : $\mathbf{S}(\mathbf{x}) = (\cos \mathbf{q} \cdot \mathbf{x}, \sin \mathbf{q} \cdot \mathbf{x}, 0)$. Note that there is no emergent magnetic field since the spin texture is coplanar. In this case, we can choose the unitary transformation $U(\mathbf{x})$ as $U(\mathbf{x}) = \sigma_z \cos(\mathbf{q} \cdot \mathbf{x}/2) + \sigma_x \sin(\mathbf{q} \cdot \mathbf{x}/2)$ to diagonalize the spin-dependent term in Eq. (1), and the resulting $U(2)$ gauge field is constant given by $\mathbf{a} = U^\dagger i\nabla U = -\mathbf{q}\sigma_y/2$. We note that \mathbf{a} cannot be gauged away even though it is constant, because it is a $U(2)$ gauge field, not $U(1)$. Since H' in this case is translationally invariant, it is easily diagonalized by the plane waves, and the resulting energy dispersion of the low-energy branch is

$$\begin{aligned} E(\mathbf{p}) &= \frac{p^2}{2m} + \frac{\hbar^2 \text{Tr } G}{2m} - \sqrt{J^2 + \frac{\hbar^2}{m^2} G_{ij} p_i p_j} \\ &= \frac{p_i g^{ij} p_j}{2m} + \frac{\hbar^2 \text{Tr } G}{2m} - J + \mathcal{O}(J^{-2}), \end{aligned} \quad (3)$$

where the repeated indices are summed over the spatial indices. Here, $G_{ij} = a_{12}^i a_{21}^j = q_i q_j / 4$ and we have defined the *effective metric* $g^{ij} = \delta^{ij} - \hbar^2 G_{ij} / (mJ)$.

The effective metric g^{ij} in Eq. (3) shows that the spin spiral suppresses the kinetic energy along \mathbf{q} at order $\mathcal{O}(J^{-1})$. This can be intuitively understood as the suppression of the hopping [17]: for large J , the itinerant electron's spin almost always aligns with the localized spins, hence the transfer integral is reduced along the varying spin directions, as indicated in Fig. 1. Correspondingly, the group velocity $dE/d\mathbf{p}$ along \mathbf{q} is reduced.

The reduction of the velocity offers a natural interpretation of the effective metric g^{ij} : we interpret it as the effective length of the real space becoming longer than it actually is. The corresponding real space metric is given by the inverse matrix of g^{ij} , which we denote by g_{ij} and is given by $g_{ij} = \delta_{ij} + \hbar^2 G_{ij}/(mJ)$ up to $\mathcal{O}(J^{-1})$. g_{ij} shows that the effective length $dl \equiv \sqrt{g_{ij} dx^i dx^j}$ along \mathbf{q} becomes longer by a factor of $1 + \hbar^2 q^2/(4mJ)$.

We emphasize that the correction to the effective metric g_{ij} appears only at $\mathcal{O}(J^{-1})$. This should be contrasted with the conventional treatments [9, 11, 15, 16, 18–20], which include an effective magnetic field or scalar potential up to $\mathcal{O}(J^0)$ but miss the effect in g_{ij} .

For general spin textures, we expect g_{ij} to vary in space, giving rise to an effectively curved space. To derive this, we write

$$H' = \begin{pmatrix} H_1 & \Lambda \\ \Lambda^\dagger & H_2 \end{pmatrix}, \quad (4a)$$

$$H_i = \mp J + (\pi_i^2 + |\mathbf{a}_{12}|^2)/2m, \quad (4b)$$

$$\Lambda = -\{\mathbf{p} - e\mathbf{A}, \mathbf{a}_{12}\}/2m, \quad (4c)$$

with $\pi_i = \mathbf{p} - e\mathbf{A} - \mathbf{a}_{ii}$, and we treat off-diagonal terms using a Schrieffer–Wolff (SW) transformation—a unitary transformation decoupling the low and high-energy subspaces. At this point, it is useful to define three length scales: (1) $l_C = \hbar/\sqrt{mJ}$, the “Compton wavelength” associated to J (we will see that $J \sim mc^2$ in a relativistic analogy), (2) $\lambda_s = |\nabla\mathbf{S}|^{-1}$, the scale over which $\mathbf{S}(\mathbf{x})$ varies, and (3) $\lambda_F \sim \hbar/\sqrt{mE}$, the wavelength of the electron at energy E . The SW transformation yields the following low-energy leading-order effective Hamiltonian:

$$\mathcal{H} = H_1 - \frac{\Lambda\Lambda^\dagger}{2J} \quad (5a)$$

$$= H_1 - \frac{\{\mathbf{p} - e\mathbf{A}, \mathbf{a}_{12}\}\{\mathbf{a}_{21}, \mathbf{p} - e\mathbf{A}\}}{8m^2J}, \quad (5b)$$

which holds for *arbitrary* spin textures in the regime

$$l_C^2 \ll \lambda_s \lambda_F, \quad (6)$$

or equivalently $\langle\Lambda\rangle \ll J$ (details in Supplemental Materials (SM)).

Furthermore, when $\mathbf{S}(\mathbf{x})$ varies sufficiently slowly such that $\lambda_s \gg \lambda_F$, the effective Hamiltonian simplifies, since derivatives of $\mathbf{a}_{12}, \mathbf{a}_{21}$ are negligible compared to the

other terms. In this regime, which we adopt henceforth, the effective Hamiltonian up to $\mathcal{O}(l_C^2/\lambda_s^2)$ is given by

$$\mathcal{H} = -J + \frac{\pi_i g^{ij} \pi_j}{2m} + V(\mathbf{x}), \quad (7)$$

where $g, V(\mathbf{x})$ are the effective metric and potential:

$$g^{ij} = \delta^{ij} - l_C^2 G_{ij}, \quad (8a)$$

$$V(\mathbf{x}) = \frac{\hbar^2 \text{Tr} G}{2m} - \frac{e\hbar l_C^2}{4m} \boldsymbol{\Omega} \cdot \mathbf{B}. \quad (8b)$$

Here, G and $\boldsymbol{\Omega}$ are the quantum metric and the Berry curvature of the real space quantum geometry, respectively. They are defined with respect to the electron's spin state aligned with the local spin at position \mathbf{R} : $(\mathbf{S}(\mathbf{R}) \cdot \boldsymbol{\sigma})|\psi_{\mathbf{R}}\rangle = |\psi_{\mathbf{R}}\rangle$. By regarding \mathbf{R} as a parameter, we define the quantum geometric tensor Q_{ij} as

$$Q_{ij} = \langle\partial_{R_i}\psi_{\mathbf{R}}|\partial_{R_j}\psi_{\mathbf{R}}\rangle - \langle\partial_{R_i}\psi_{\mathbf{R}}|\psi_{\mathbf{R}}\rangle\langle\psi_{\mathbf{R}}|\partial_{R_j}\psi_{\mathbf{R}}\rangle \quad (9)$$

We can readily show $Q_{ij} = a_{12}^i a_{21}^j$, and G and $\boldsymbol{\Omega}$ are given by $G_{ij} = \text{Re} Q_{ij}$ and $\Omega^i = -\epsilon^{ijk} \text{Im} Q_{jk}$. G can also be written with $\mathbf{S}(\mathbf{x})$ as $G_{ij} \equiv \frac{1}{4}(\partial_i\mathbf{S}) \cdot (\partial_j\mathbf{S})$. We can verify that the Hamiltonian (7) reduces to Eq. (3) for a spin spiral with uniform metric g .

Real space quantum geometry naturally enters the effective Hamiltonian (7) in two ways. The first is through the effective potential $V(\mathbf{x})$, whose leading $\mathcal{O}(l_C^0)$ term is proportional to $\text{Tr} G \propto |\nabla\mathbf{S}|^2$ [9] and corresponds to the “geometric potential” in literature [18–20]. The subleading $\mathcal{O}(l_C^2)$ term in $V(\mathbf{x})$ represents orbital magnetization coupling to the external \mathbf{B} field.

Interestingly, quantum geometry also manifests in a second way: through the effective metric g^{ij} . The quantum metric G_{ij} directly modifies the spatial metric g^{ij} and thereby influences electrons' motion. The inverse of g^{ij} , denoted by g_{ij} , defines the effective line element $dl = \sqrt{g_{ij} dx^i dx^j}$, and thus a spatially varying quantum metric leads to an effective curved space, i.e., *emergent gravitational field* [21]. The effect of the emergent curved space scales as $\mathcal{O}(l_C^2/\lambda_F^2) \sim \mathcal{O}(E_K/J)$, in close analogy with true (post-Newtonian/Einstein) gravitational effects scaling as $\mathcal{O}(E_K/mc^2)$, where E_K is the kinetic energy of a particle of mass m and c is the speed of light. Hence $J \sim mc^2$ in this analogy, which we make precise using a Lagrangian formulation in SM.

Importantly, the emergent curved space associated with the spatial metric g gives rise to physical effects that cannot be captured by a scalar potential. This parallels how Einstein's theory of gravity goes beyond Newtonian gravity. We now discuss physical consequences of the emergent gravitational field that are qualitatively new.

Gravitational lensing. — To understand the physical effects of $g(\mathbf{x})$, we analyze the classical equations of mo-

tion of the electrons, given by Hamilton's equations:

$$\dot{x}^i = \frac{\partial \mathcal{H}}{\partial p_i} = \frac{g^{ij} \pi_j}{m}, \quad (10a)$$

$$\dot{p}_i = -\frac{\partial \mathcal{H}}{\partial x^i} = -\frac{1}{2m} \pi_j \frac{\partial g^{jk}}{\partial x^i} \pi_k + \frac{e}{m} \frac{\partial \mathcal{A}_j}{\partial x^i} g^{jk} \pi_k - \frac{\partial V}{\partial x^i}, \quad (10b)$$

where $\mathcal{A} = \mathbf{A} + (\hbar/e)\mathbf{a}_{11}$ is the total effective vector potential, including the external and emergent gauge fields. Taking the time derivative of Eq. (10a) and using Eq. (10b), we find

$$m(\ddot{x}^i + \Gamma_{jk}^i \dot{x}^j \dot{x}^k) = F^i, \quad (11)$$

where $\Gamma_{jk}^i = (g^{il}/2)(\partial_j g_{kl} + \partial_k g_{jl} - \partial_l g_{jk})$ is the Christoffel symbol with g_{ij} the inverse of g^{ij} . $F^i = g^{ij}(e\mathcal{B}_{jk}\dot{x}^k - \partial_j V)$ is the force from the potential V and the total magnetic field $\mathcal{B}_{jk} = \partial_j \mathcal{A}_k - \partial_k \mathcal{A}_j$. The term with Γ_{jk}^i scales as $\mathcal{O}(l_C^2/\lambda_s^2)$ and captures the effects of the emergent curved space. Notably, the electron feels a force proportional to the square of its velocity.

For constant effective potential V and zero magnetic field \mathcal{B} , the right hand side of Eq. (11) vanishes, yielding the geodesic equation: $\ddot{x}^i + \Gamma_{kl}^i \dot{x}^k \dot{x}^l = 0$. The electron thus follows a geodesic in the curved space in this case. For constant metrics, Γ_{jk}^i vanishes and the solutions are straight lines, while for spatially varying metrics, $\Gamma_{jk}^i \neq 0$ and thus the geodesics are no longer straight lines in general, i.e., the emergent curved space bends the trajectory. Notably, such trajectories are independent of the particle's initial velocity up to a rescaling of time: if $\mathbf{x}(t)$ is a geodesic, so is $\mathbf{x}(\alpha t)$ for an arbitrary constant α . Therefore, the effects of g persist even for fast-moving particles. This is in sharp contrast with the force from a potential V , which is independent of velocity and thus affects fast-moving particles less than slow particles. This is analogous to how the trajectory of light is affected by a curved space-time metric (Einstein gravity) but not by a scalar potential (Newtonian gravity).

Let us discuss perhaps the simplest consequence of the emergent curved space: the bending of electron trajectories between domains of distinct spin orders. For instance, suppose $\mathbf{S}(\mathbf{x}) = \hat{z}$ in the region $x \rightarrow -\infty$ and $\mathbf{S}(\mathbf{x}) = (0, \sin \frac{2\pi x}{\lambda_s}, \cos \frac{2\pi x}{\lambda_s})$ in the region $x \rightarrow +\infty$, in two spatial dimensions. This describes the transition between ferromagnetic and helical domains, which could be realized for instance in a material with the Dzyaloshinskii-Moriya interaction. The emergent metric is trivially $g^{ij} = \delta^{ij}$ in the ferromagnetic region, while g^{xx} receives a correction $g^{xx} = 1 - (\pi l_C/\lambda_s)^2$, in the helical region. The resulting electron motion can be worked out using the conservation of energy $E = mg_{ij}\dot{x}^i \dot{x}^j/2$ and conservation of y -momentum $p_y = mg_{yi}\dot{x}^i$. We ignore the potential V for now. This can be justified, for instance, by electrostatic gating in the helical region. Then, letting

$\theta_{L/R}$ denote the angles of a geodesic with respect to the x -axis in the left and right regions, respectively, one finds

$$\frac{\tan \theta_R}{\tan \theta_L} = \sqrt{1 + (\pi l_C/\lambda_s)^2}. \quad (12)$$

This describes the bending of electrons towards the normal as they pass from the ferromagnetic region to the helical region. In contrast with Snell's law $\sin \theta_R/\sin \theta_L = n_L/n_R$ for light, there is no condition for total internal reflection. This effect remains even in the presence of the potential V , and admits interesting generalizations, for instance to the case of domain walls between distinct spiral phases, which we discuss in SM.

Next, as a simple and solvable example, we consider the spin texture which we call the *radial spiral*

$$\mathbf{S}(\mathbf{x}) = (\cos \frac{2\pi r}{\lambda_s}, \sin \frac{2\pi r}{\lambda_s}, 0), \quad (13)$$

where $r = |\mathbf{x}|$ is the radial coordinate. Locally, the radial spiral approximates configurations minimizing the spin gradient energy $(\partial_i \mathbf{S})^2$ under radial boundary conditions $\mathbf{S}(r_{\min}) \neq \mathbf{S}(r_{\max})$. Globally, the radial spiral is the unique continuous, rotationally symmetric, coplanar spin texture with constant $V(\mathbf{x})$ (see SM for more details).

The radial spiral is depicted in Fig. 2. It satisfies $\mathbf{b} = 0$, $V(\mathbf{x}) = \hbar^2/8m\lambda_s^2$, and

$$g^{ij} = \delta^{ij} - \left(\frac{\pi l_C}{\lambda_s}\right)^2 \frac{x^i x^j}{r^2}. \quad (14)$$

Electron motion is thus described simply by the geodesic equation, which takes the form

$$\ddot{\mathbf{x}} = -\left(\frac{\pi l_C}{\lambda_s}\right)^2 \frac{(\dot{\mathbf{x}} \times \mathbf{x})^2 \mathbf{x}}{x^4}, \quad (15)$$

indicating an $\mathcal{O}(l_C^2/\lambda_s^2)$ correction to free-particle motion. The geodesics are $r(t) = \pm \sqrt{(v_0 t + r_0)^2 + (\xi \hbar t / r_0)^2}$, $\theta(t) = \theta_0 + (\tan^{-1}(\gamma t + \delta) - \tan^{-1} \delta) / \xi$ in polar coordinates with $\xi = \sqrt{1 - (\pi l_C/\lambda_s)^2}$, where $h = r^2 \dot{\theta}$ is a conserved angular momentum, $(r(0), \dot{r}(0), \theta(0)) = (r_0, v_0, \theta_0)$, $\gamma = (h\xi/r_0^2)(1 + \delta^2)$ and $\delta = r_0 v_0 / (h\xi)$. Alternatively, the geodesics can be expressed as straight lines in coordinates which trivialize the metric, as shown in SM. An example trajectory is plotted in Fig. 2, showing clearly the *lensing* of the electron geodesic.

The properties of geodesics in the previous two examples can be elucidated by a geometric perspective. Quite generally, the emergent curved space in d spatial dimensions corresponds to that of a surface embedded in higher dimensions. This follows from the effective line element $dl = \sqrt{g_{ij} dx^i dx^j}$, which can be rewritten as

$$dl^2 = d\mathbf{x}^2 + l_C^2 G_{ij} dx^i dx^j = d\mathbf{x}^2 + l_C^2 ds^2. \quad (16)$$

Here, $ds = \sqrt{G_{ij} dx^i dx^j}$ defines the quantum distance via the quantum metric G_{ij} in the local Hilbert space,

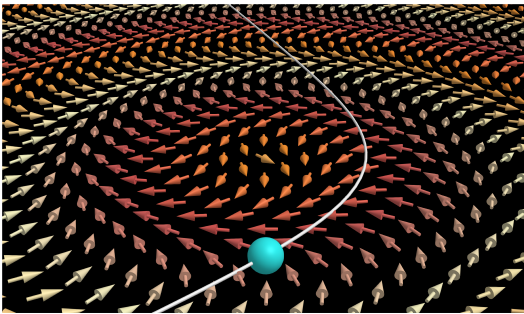


FIG. 2. The radial spiral spin texture (Eq. (13)) and a corresponding electron geodesic (solid curve). The effectively curved space gives rise to gravitational lensing of electrons around the origin.

which is $\mathbb{C}P^1 \simeq S^2$ in our case. The effective line element Eq. (16) thus corresponds to a d -dimensional surface embedded in the $(d+2)$ -dimensional manifold, $\mathbb{R}^d \times \mathbb{C}P^1$, with l_C the length scale of the extra dimensions. For coplanar textures such as $\mathbf{S}(\mathbf{x}) = (\cos \theta(\mathbf{x}), \sin \theta(\mathbf{x}), 0)$, the electron's spin is restricted to a one-dimensional subspace, and the effective curved space is a surface in $d+1$ dimensions. The effective line element is given by

$$dl^2 = d\mathbf{x}^2 + \frac{l_C^2}{4} d\theta^2 = d\mathbf{x}^2 + dz_{\text{eff}}^2, \quad (17)$$

whose geometry is the d -dimensional surface defined by $(x^1, \dots, x^d, z_{\text{eff}}(\mathbf{x}))$ with $z_{\text{eff}} = l_C \theta(\mathbf{x})/2$.

From this geometric perspective, the metric and geodesics of the ferromagnet-to-helical transition discussed above correspond to the geometry of two half-planes joined at $x=0$, with $z_{\text{eff}}=0$ and $z_{\text{eff}}=\pi l_C x/\lambda_s$ in the left and right regions, respectively. For the radial spiral, the metric and the geodesics correspond to the geometry of a cone with $z_{\text{eff}} = \pi l_C r/\lambda_s$. Incidentally, the cone geometry Eq. (14) is the solution of the Einstein equations with a point mass M in $(2+1)$ -dimensions with the identification $(\pi l_C/\lambda_s)^2 \sim 8GM/c^2$ where G is the gravitational constant [22]. The radial spiral therefore realizes the simplest non-vacuum solution of $(2+1)d$ Einstein gravity with vanishing cosmological constant. More general spin textures generically yield more complex metrics and geodesics. We collectively refer to the ensuing new effects on electronic motion as *gravitational lensing*. Crucially, gravitational lensing becomes stronger for faster electrons and cannot be explained by an effective magnetic or electric field.

Curvature of the effective curved space is essential in gravitational lensing. In flat space with zero curvature, there exist coordinates where geodesics, i.e., trajectories of free-particle motion, are straight lines, and any two geodesics can intersect at most once. Thus, multiple intersections between geodesics require finite curvature in the effective space.

In two-dimensional systems, this observation is for-

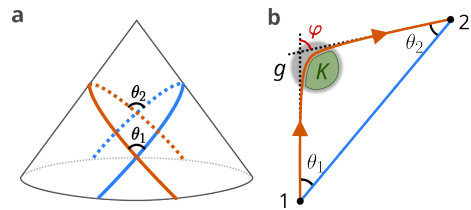


FIG. 3. (a) Two geodesics on a cone. (b) Deflection due to gravitational lensing when the curved metric and the curvature are localized in a gray region. The deflection angle φ is given by the curvature K enclosed by the blue and orange lines.

malized with the Gauss-Bonnet theorem, which relates a closed loop on a curved surface to the Gaussian curvature enclosed by the loop [23, 24]. For a polygon S made of geodesics on a curved surface, the following relation follows from the Gauss-Bonnet theorem:

$$\sum_i \phi_i + K = \sum_i (\pi - \theta_i) + K = 2\pi, \quad (18)$$

where i is the label for the vertices, ϕ_i and $\theta_i = \pi - \phi_i$ are the exterior and interior angle at vertex i , and K is the integrated Gaussian curvature enclosed by the polygon:

$$K = \int_S \kappa \sqrt{\det g_{ij}} d^2x. \quad (19)$$

Here, $\kappa = R_{xyxy}/\det g_{ij}$ is the Gaussian curvature and R_{ijkl} is the Riemann curvature tensor for the effective metric g_{ij} (see SM). We note that R_{ijkl} can be expressed in terms of the Riemann curvature of the Hilbert space defined by the quantum metric, as detailed in SM. For the coplanar texture Eq. (17), this takes the form

$$K = \int d^2x \frac{l_C^2}{4} \frac{(\partial_x^2 \theta)(\partial_y^2 \theta) - (\partial_x \partial_y \theta)^2}{(1 + |l_C \partial_i \theta / 2|^2)^{3/2}}. \quad (20)$$

When the metric is trivial and the curvature vanishes, $K=0$ and Eq. (18) reduces to the well-known polygon exterior angle sum theorem. On a curved surface, K is finite, and the exterior angle sum will be modified.

Eq. (18) applies when two geodesics intersect at two points as in Fig. 3(a), since they form a two-edged polygon. In this case, Eq. (18) reduces to

$$\theta_1 + \theta_2 = K. \quad (21)$$

It should be emphasized that θ_i is measured using the effective metric g_{ij} , and may differ from the usual angle defined by the trivial metric δ_{ij} . For the radial spiral, θ_i 's are measured on the corresponding cone, as shown in Fig. 3. The curvature vanishes except at the origin, which contributes to K by the angle deficit of the cone: $\kappa = 2\pi(1 - 1/\sqrt{1 + (\pi l_C/\lambda_s)^2})\delta(\mathbf{x})$.

More generally, the deflection angle is related to the curvature. Consider the case where the curved metric

(and thus the curvature) is localized in a small region, as shown in Fig. 3(b), and a particle travels from point 1 to point 2 on a geodesic (orange line). If the points are sufficiently far away from the curved region, we can also connect the points only through the flat space with a geodesic, which is a straight line (blue line). Then we can define the deflection angle φ as the angle change of the velocity from point 1 to 2 within the flat region. On the other hand, since the orange and blue lines form a geodesic polygon, we can apply Eq. (21). Since the deflection angle is given by $\varphi = \theta_1 + \theta_2$, it follows that $\varphi = K$. Note that φ here is the angle change of the velocity measured at points 1 and 2 within the flat space, and thus is defined with the flat metric δ_{ij} . This relation reveals the geometric nature of the gravitational lensing [25].

For example, we may consider a coplanar texture varying with wavelength λ_s . From Eq. (20), the deflection angle over a region of area A scales as $\varphi \sim Al_C^2/\lambda_s^4$. For masses ranging from 0.1 to 1 electron mass and typical 10-100 meV Hund's couplings, $l_C \sim 1$ -10 nm, while typical spin textures have $\lambda_s \sim 10$ -100 nm. Thus, the deflection angle from gravitational lensing is within the observable range over areas $A \sim \lambda_s^2$, and can be enhanced by coherent electron motion across larger samples.

Discussion. — The emergent curved space we proposed originates from the quantum nature of electrons. Indeed, the spatial metric correction vanishes as $\hbar \rightarrow 0$. It can also be interpreted through the electron's wave nature. The effective metric g determines the electron's wavelength λ for a given frequency ω , and thus plays the role of the refractive index. A spatially varying g corresponds to a spatially dependent refractive index, and thus causes refraction, i.e., the lensing effect. We note that gravitational lensing of light in general relativity can also be understood with an effective refractive index [14].

It is important to note that the emergent curved space — and thus the gravitational lensing — does not require any symmetry breaking. This contrasts with the emergent magnetic field, which requires the time reversal symmetry breaking. In particular, gravitational lensing can occur without magnetic fields in contrast to the conventional electron lensing in electron microscopes [26], where magnetic fields are used to control electrons' trajectory. Gravitational lensing does not require noncoplanar spin textures either, as we demonstrated with the radial spiral. This is in sharp contrast to emergent magnetic field [1–6].

A similar gravitational picture is expected to hold for general systems described by a Hamiltonian of the form (2) with $SU(2)$ gauge fields, under assumptions analogous to $l_C^2 \ll \lambda_s \lambda_F$ and $\lambda_s \gg \lambda_F$. For instance, the spin degrees σ can be replaced with a pseudo-spin. We also note that our assumptions on the length scales allow only perturbatively small gravitational fields ($|g_{ij} - \delta_{ij}| \ll 1$). Exploring analogues of strong gravitational effects in a similar setup, such as a black hole,

would be an interesting future direction.

A curved space was discussed in contexts of condensed matter previously. For example, strain responses or deformation effects [27–32] and phonon scattering by a vortex [33] were discussed with a curved space picture. Weyl semimetals with inhomogeneous tilt of the Weyl cone, which may be induced by strain or external fields, were also studied in analogy with the curved spacetime [34–41] and gravitational lensing [42, 43]. We emphasize, however, that the emergent curved space proposed here does *not* require external strain or nontrivial band structure. It emerges due to the quantum mechanical coupling between itinerant electrons and localized spins, and would be potentially as diverse as the spin textures, offering rich platforms. The dynamics of spin textures [44–48] may further lead to time-dependent curved space, such as a gravitational wave analog [49], which we leave for future study. A curved space is also used as a theoretical tool to study electronic systems, such as fractional quantum Hall systems [27, 50, 51]. The emergent curved space may provide a method to experimentally test these theoretical results.

The concept of emergent gauge field is so far well established and generically appears in various quantum systems. In these systems, there should always be a correction due to the finite energy gap, which results in emergent gravitational fields. Therefore, we expect emergent curved space to appear in quantum systems ubiquitously.

YO thanks Filippo Gaglioli for encouraging discussion. LF and NP thank Aidan Reddy for participation in a related project. This work was supported by the Air Force Office of Scientific Research under award number FA2386-24-1-4043. LF was supported in part by the Simons Investigator Award from the Simons Foundation.

SUPPLEMENTAL MATERIALS

Derivation of the effective Hamiltonian

Effective Hamiltonian for general spin textures

Consider the following Hamiltonian:

$$H = \frac{(\mathbf{p} - e\mathbf{A})^2}{2m} - J\mathbf{S}(\mathbf{x}) \cdot \boldsymbol{\sigma} \quad (22)$$

Here, we include the spatial dependence of J . In this section, assuming J is large, we derive the low-energy effective theory up to $\mathcal{O}(J^{-1})$ by applying the Schrieffer-Wolff transformation.

We first consider the unitary matrix $U(\mathbf{x})$ that diagonalizes the spin:

$$U^\dagger(\mathbf{x})(\mathbf{S}(\mathbf{x}) \cdot \boldsymbol{\sigma})U(\mathbf{x}) = \sigma_z \quad (23)$$

Then we can obtain Hamiltonian H' in the new basis defined by $U(\mathbf{x})$:

$$H' = U^\dagger(\mathbf{x})HU(\mathbf{x}) = \frac{(\mathbf{p} - e\mathbf{A} - \mathbf{a})^2}{2m} - J\sigma_z \quad (24)$$

where we set $\hbar = 1$, and \mathbf{a} is defined as

$$\mathbf{a} = U^\dagger(\mathbf{x})i\nabla U(\mathbf{x}) = \begin{pmatrix} \mathbf{a}_{11} & \mathbf{a}_{12} \\ \mathbf{a}_{21} & \mathbf{a}_{22} \end{pmatrix} \quad (25)$$

and serves as a $U(2)$ gauge field. From now on, we include $(\mathbf{a}_{11} + \mathbf{a}_{22})/2$ in the regular vector potential \mathbf{A} and treat \mathbf{a} as a $SU(2)$ gauge field with $\mathbf{a}_{11} + \mathbf{a}_{22} = 0$. Noting that $\mathbf{a}_{12} = \mathbf{a}_{21}^*$, H' can be written as

$$H' = H_0 + V \quad (26)$$

where

$$H_0 = \begin{pmatrix} H_1 & 0 \\ 0 & H_2 \end{pmatrix} \quad (27a)$$

$$V = \begin{pmatrix} 0 & \Lambda \\ \Lambda^\dagger & 0 \end{pmatrix} \quad (27b)$$

$$\Lambda = -\frac{1}{2m}\{\boldsymbol{\pi}_0, \mathbf{a}_{12}\} \quad (27c)$$

Here, $H_i = (\boldsymbol{\pi}_i^2 + |\mathbf{a}_{12}|^2)/(2m) \mp J$, $\boldsymbol{\pi}_i = \mathbf{p} - e\mathbf{A} - \mathbf{a}_{ii}$, and $\boldsymbol{\pi}_0 = \mathbf{p} - e\mathbf{A}$. It may be worth noting that Λ has a similar form to the strain generator $J_\nu^\mu \equiv \{x^\mu, p_\nu\}$ [29, 31]. When \mathbf{a}_{12} is linear in the position x^i and $\mathbf{A} = 0$, then Λ coincides with the strain generator up to a factor. For more general \mathbf{a}_{12} , Λ can be interpreted as a generator for a position-dependent strain.

We now apply Schrieffer–Wolff transformation to H' assuming that J is large. We consider a unitary transformation e^S to apply to H' as $H'' = e^S H' e^{-S}$. Assuming

that $S = S^{(1)} + S^{(2)} + \dots$ with $S^{(i)} = \mathcal{O}((\Lambda/J)^i)$, H'' is expanded as

$$\begin{aligned} H'' &= H' + [S, H'] + \frac{1}{2}[S, [S, H']] + \dots \\ &= H_0 + V + [S, H_0] + [S, V] + \frac{1}{2}[S, [S, H_0]] + \dots \end{aligned} \quad (28)$$

We require $S^{(1)}$ to satisfy the following:

$$V + [S^{(1)}, H_0] = 0. \quad (29)$$

Writing each element explicitly,

$$S_{11}^{(1)} H_1 - H_1 S_{11}^{(1)} = 0, \quad (30a)$$

$$\Lambda + S_{12}^{(1)} H_2 - H_1 S_{12}^{(1)} = 0, \quad (30b)$$

$$\Lambda^\dagger + S_{21}^{(1)} H_1 - H_2 S_{21}^{(1)} = 0, \quad (30c)$$

$$S_{22}^{(1)} H_2 - H_2 S_{22}^{(1)} = 0. \quad (30d)$$

For the leading order in Λ/J , these can be solved as

$$S_{12}^{(1)} = -S_{21}^{(1)\dagger} = -\frac{\Lambda}{2J}, \quad (31)$$

$$S_{11}^{(1)} = S_{22}^{(1)} = 0. \quad (32)$$

Then the effective Hamiltonian for the low energy sector up to $\mathcal{O}(J^{-1})$ is given by $H_{\text{eff}} = H''_{11}$ as

$$\begin{aligned} H_{\text{eff}} &= -J + \frac{\boldsymbol{\pi}_1^2 + |\mathbf{a}_{12}|^2}{2m} - \frac{\Lambda\Lambda^\dagger}{2J} \\ &= -J + \frac{\boldsymbol{\pi}_1^2 + |\mathbf{a}_{12}|^2}{2m} - \frac{\{\boldsymbol{\pi}_0, \mathbf{a}_{12}\}\{\mathbf{a}_{21}, \boldsymbol{\pi}_0\}}{8m^2 J} \end{aligned} \quad (33)$$

As we discussed in the main text, this effective Hamiltonian is valid when $l_C^2 \ll \lambda_s \lambda_F$ with $l_C \equiv 1/\sqrt{mJ}$, the length scale of the spin texture $\lambda_s \equiv |\nabla \mathbf{S}|^{-1}$, and the Fermi wavelength λ_F .

When the spin is slowly varying in space

When the length scale of spatial variation of $\mathbf{S}(\mathbf{x})$, denoted as λ_s , is large so that $\lambda_s \gg \lambda_F$, the derivative of \mathbf{a}_{12} in Eq. (33) is negligible compared to the other terms. Therefore, we can further simplify Eq. (33) as

$$\begin{aligned} H_{\text{eff}} &= -J + \frac{\boldsymbol{\pi}_1^2 + |\mathbf{a}_{12}|^2}{2m} - \frac{\pi_{0i} Q_{ij} \pi_{0j}}{2m^2 J} + \mathcal{O}\left(E_F \frac{\lambda_F l_C^2}{\lambda_s^3}\right) \\ &= -J + \frac{\boldsymbol{\pi}_1^2 + |\mathbf{a}_{12}|^2}{2m} - \frac{\pi_{0i} G_{ij} \pi_{0j}}{2m^2 J} - \frac{e\hbar^3}{4m^2 J} \boldsymbol{\Omega} \cdot \mathbf{B} \end{aligned} \quad (34)$$

where $Q_{ij} = a_{12}^i a_{21}^j$ is the quantum geometric tensor, $G_{ij} = \text{Re} Q_{ij}$, $\Omega_{ij} = -2 \text{Im} Q_{ij}$ are the quantum metric and the Berry curvature respectively, and $\boldsymbol{\Omega}$ is defined as

$\Omega^i = \epsilon^{ijk}\Omega_{jk}/2$. E_F is the Fermi energy. Since $\mathbf{a}_{11} = \mathcal{O}(1/\lambda_s)$ and $G_{ij} = \mathcal{O}(1/\lambda_s^2)$, we can replace $\boldsymbol{\pi}_0$ with $\boldsymbol{\pi}_1$ up to the same accuracy of the approximation to obtain

$$H_{\text{eff}} = -J(\mathbf{x}) + \frac{\pi_{1i}g^{ij}\pi_{1j}}{2m} + \frac{\hbar^2 \text{Tr} G}{2m} - \frac{e^3\hbar}{4m^2J}\boldsymbol{\Omega} \cdot \mathbf{B} + \mathcal{O}\left(E_F \frac{\lambda_F l_C^2}{\lambda_s^3}\right) \quad (35)$$

Here, $g^{ij} = \delta^{ij} - l_C^2 G_{ij}$ is the effective metric, and $\boldsymbol{\Omega} = \nabla \times \mathbf{a}_{11}$ is the Berry curvature.

Analogy to true gravity

The emergent gravity is an analogue of Einstein gravity in condensed matter. This analogy becomes clearer in the Lagrangian formalism. The Lagrangian corresponding to the effective Hamiltonian in the main text is given by $L = p_i \dot{x}^i - \mathcal{H}$ as

$$L(x, \dot{x}) = \frac{m}{2} g_{ij}(\mathbf{x}) \dot{x}^i \dot{x}^j + e\mathcal{A}_i(\mathbf{x}) \dot{x}^i + J - V(\mathbf{x}) \quad (36)$$

This Lagrangian can be obtained from the following action up to $\mathcal{O}(J^{-1}\lambda_s^{-2})$:

$$S = S_0 + m\tilde{c} \int \sqrt{\tilde{g}_{\mu\nu} dx^\mu dx^\nu} \quad (37)$$

Here, $S_0 = \int dt (m\dot{x}^2/2 - V + e\mathcal{A}_i \dot{x}^i)$ is the Lagrangian for a particle in a flat space-time with potential V and vector potential \mathcal{A}_i . The second term in Eq. (37) represents the effect of the emergent gravity, where μ and ν run over 0 to 3, $(x^0, x^1, x^2, x^3) = (\tilde{c}t, x, y, z)$. \tilde{c} is defined through $m\tilde{c}^2 = J$. The space-time metric \tilde{g} is given by

$$\tilde{g}_{\mu\nu} = \begin{pmatrix} 1 & \\ & \frac{\hbar^2}{m^2 \tilde{c}^2} G_{\mu\nu} \end{pmatrix} \quad (38)$$

Eq. (37) shows that the correction to our low-energy effective action takes the same form as the action for a particle with the space-time metric \tilde{g} . The role of the rest energy mc^2 in the true gravity with c the speed of light is played by $J = m\tilde{c}^2$ in the emergent gravity, defining an effective speed of light \tilde{c} . The effect from the spatial components of the space time metric gives the correction to the Hamiltonian of order $\mathcal{O}(E_F/(m\tilde{c}^2))$, just as the true gravity effects from the curved space-time scales as $\mathcal{O}(E_K/(mc^2))$ with E_K the kinetic energy of a particle.

Correspondence to other forms of Hamiltonian in a curved space

In the main text, we discuss the effective Hamiltonian in the following form as the Hamiltonian in a curved space:

$$H^{(1)} = \frac{p_i g^{ij} p_j}{2m} + V(\mathbf{x}) \quad (39)$$

In literature, there is another form of the Hamiltonian which also describes an electron in curved space given by

$$H^{(2)} = \frac{1}{2m} \frac{1}{\sqrt{g}} p_i (\sqrt{g} g^{ij} p_j) + V(\mathbf{x}) \quad (40)$$

where $g = \det g_{ij}$. The latter is obtained by replacing the Laplacian in the Hamiltonian in flat space with the one in a curved space. In this section, we show that these are equivalent up to the accuracy we discussed in the main text.

The most important difference between Eq. (39) and (40) is the normalization of the wavefunction $\psi(\mathbf{x})$ they assume. In the main text, we always assume that the wavefunction is normalized in the following way:

$$\int d^d x |\psi^{(1)}(\mathbf{x})|^2 = 1 \quad (41)$$

On the other hand, the Hamiltonian $H^{(2)}$ implicitly assumes that the wavefunction is normalized as follows:

$$\int d^d x \sqrt{g} |\psi^{(2)}(\mathbf{x})|^2 = 1 \quad (42)$$

These two conventions are related as follows: the solution of the Schrodinger equation under $H^{(1)}$, $\psi^{(1)}$, is related to the one under $H^{(2)}$, $\psi^{(2)}$, as $\psi^{(1)} = g^{1/4} \psi^{(2)}$. Since g depends on position in general, the states $\psi^{(1)}$ and $\psi^{(2)}$ and their corresponding Hamiltonian look different from each another.

To show their equivalence, we formulate the Schrodinger equation in a variational way. The Schrodinger equation under Hamiltonian $H^{(i)}$ is obtained from the following action:

$$S^{(1)}[\psi] = \int dt d^d x \left[i\psi^* \frac{\partial \psi}{\partial t} - \frac{1}{2m} (p_i \psi)^* g^{ij} (p_j \psi) - V|\psi|^2 \right] \quad (43)$$

$$S^{(2)}[\psi] = \int dt d^d x \sqrt{g} \left[i\psi^* \frac{\partial \psi}{\partial t} - \frac{1}{2m} (p_i \psi)^* g^{ij} (p_j \psi) - V|\psi|^2 \right] \quad (44)$$

where we have set $\hbar = 1$. We find the Schrodinger equation under $H^{(i)}$ by requiring $S^{(i)}$ to be stationary under arbitrary variations of ψ and ψ^* : $\delta S^{(i)}/\delta \psi^* = 0$, and its complex conjugate.

Now we would like to show that $S^{(1)}[g^{1/4}\psi] = S^{(2)}[\psi]$ up to the accuracy we considered in the main text. We start with $S^{(1)}[g^{1/4}\psi]$ and rewrite it as follows:

$$S^{(1)}[g^{1/4}\psi] = \int dt d^d x \sqrt{g} \left[i\psi^* \frac{\partial \psi}{\partial t} - V|\psi|^2 - \frac{1}{2m} (g^{-1/4} p_i g^{1/4} \psi)^* g^{ij} (g^{-1/4} p_j g^{1/4} \psi) \right] \quad (45)$$

Here, we have assumed g is time-independent. Noting $g^{-1/4}p_i g^{1/4} = p_i - i\alpha_i$ with $\alpha_i = (1/4)\partial_i \log g$, we can rewrite $S^{(1)}[g^{1/4}\psi]$ as

$$\begin{aligned} S^{(1)}[g^{1/4}\psi] &= \int dt d^d x \sqrt{g} \left[i\psi^* \frac{\partial \psi}{\partial t} - V|\psi|^2 \right. \\ &\quad \left. - \frac{1}{2m} ((p_i - i\alpha_i)\psi)^* g^{ij} ((p_j - i\alpha_j)\psi) \right] \\ &= S^{(2)}[\psi] + \int dt d^d x \sqrt{g} \frac{1}{2m} (\partial_i \alpha^i - \alpha^i \alpha_i) |\psi|^2 \end{aligned} \quad (46)$$

where $\alpha^i = g^{ij}\alpha_j$. Eq. (46) shows that the theory (39) differs from the theory (40) only by a correction to a potential, $\delta V = (\partial_i \alpha^i - \alpha^i \alpha_i)/(2m)$.

Lastly, we note that the metric g we considered in the main text is $g_{ij} = \delta_{ij} + \mathcal{O}(l_C^2 \lambda_s^{-2})$ with $l_C = (mJ)^{-1/2}$ the coupling constant and λ_s the length scale of the spin texture. Therefore, $\alpha = \mathcal{O}(l_C^2 \lambda_s^{-3})$ and thus the last term in Eq. (46) is $\mathcal{O}(l_C^2 \lambda_s^{-4})$. Then we find

$$S^{(1)}[g^{1/4}\psi] = S^{(2)}[\psi] + \mathcal{O}(l_C^2 \lambda_s^{-4}). \quad (47)$$

Therefore, $H(1)$ and $H^{(2)}$ are equivalent up to $\mathcal{O}(l_C^2 \lambda_s^{-4})$.

Geodesics in spin textures

In this section, we provide more details on the various spin textures explored in the main text and extensions thereof.

Radial spiral spin texture

Here, we present details on the radial spiral spin texture

$$\mathbf{S}(\mathbf{x}) = \left(\cos \frac{2\pi}{\lambda_s} r, \sin \frac{2\pi}{\lambda_s} r, 0 \right), \quad (48)$$

where $r = \sqrt{x^2 + y^2}$, a simple spin texture with constant real-space quantum metric and $\mathbf{b} = 0$. This combination of features implies that only the emergent gravitational field

$$g^{ij} = \delta^{ij} - \nu \frac{x^i x^j}{r^2}. \quad (49)$$

enters the electron equation of motion. Here we've defined

$$\nu = (\pi l_C / \lambda_s)^2. \quad (50)$$

Geodesics from direct calculation

The geodesic equation $\ddot{x}^i + \Gamma_{jk}^i \dot{x}^j \dot{x}^k = 0$ reduces to

$$\ddot{\mathbf{x}} = -\nu \mathbf{x} \frac{(\dot{\mathbf{x}} \times \mathbf{x})^2}{x^4}. \quad (51)$$

In radial coordinates, this is

$$\ddot{\mathbf{r}} = -\nu r \dot{\theta}^2 \hat{\mathbf{r}}. \quad (52)$$

Comparing with

$$\ddot{\mathbf{r}} = (\ddot{r} - r\dot{\theta}^2)\hat{\mathbf{r}} + \frac{d}{dt}(r^2\dot{\theta})\hat{\boldsymbol{\theta}}, \quad (53)$$

we find two scalar equations:

$$0 = \frac{d}{dt}(r^2\dot{\theta}) \quad (54a)$$

$$\ddot{r} = (1 - \nu)r\dot{\theta}^2. \quad (54b)$$

We may define a conserved angular momentum $h = r^2\dot{\theta} = \text{constant}$. The remaining equation is

$$\ddot{r} = (1 - \nu)h^2/r^3. \quad (55)$$

Assuming $r(0) = r_0$ and $\dot{r}(0) = v_0$, we have

$$r(t) = \pm \sqrt{(v_0 t + r_0)^2 + (1 - \nu)(ht/r_0)^2}. \quad (56)$$

We can integrate to find $\theta(t)$ using $\dot{\theta} = h/r^2$. Let $\theta(0) = \theta_0$. We find

$$\begin{aligned} \theta(t) - \theta_0 &= \\ &= \frac{1}{\sqrt{1 - \nu}} \left(\tan^{-1} \left(\left[\frac{v_0^2}{h\sqrt{1 - \nu}} + \frac{h\sqrt{1 - \nu}}{r_0^2} \right] t + \frac{r_0 v_0}{h\sqrt{1 - \nu}} \right) \right. \\ &\quad \left. - \tan^{-1} \left(\frac{r_0 v_0}{h\sqrt{1 - \nu}} \right) \right) \end{aligned} \quad (57)$$

This describes a particle on a cone, with the conical singularity at $r = 0$. This geometry also describes the solution of the Einstein equations in the presence of a point mass in (2+1)d with zero cosmological constant [22]. Note that there is no Newtonian attraction; a geodesic at fixed $r(t) = r_0$ is perfectly valid. However, there is "focusing"; two trajectories which pass on either side of the origin will intersect on the other side.

At this point, geodesics depend on the independent parameters (r_0, θ_0, v_0, h) . Another useful form is in terms of $(r_0, \theta_0, v_i, \phi_0)$ where

$$\mathbf{v}_i = v_i (\cos \phi_0, \sin \phi_0) \quad (58)$$

is the initial Cartesian velocity. The conserved angular momentum is

$$h = r_0 v \sin(\phi_0 - \theta_0), \quad (59)$$

while the initial radial velocity v_0 satisfies

$$v_0^2 = v_i^2 \cos^2(\phi_0 - \theta_0). \quad (60)$$

We rescale time $t \mapsto t/v_i$ in the following, which omits explicit dependence on velocity. Defining the angle difference

$$\vartheta_0 = \phi_0 - \theta_0, \quad (61)$$

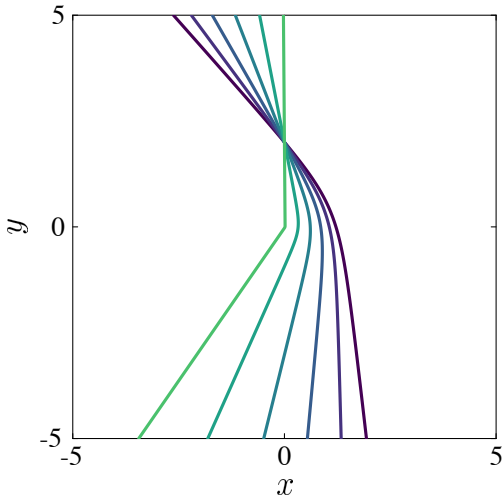


FIG. 4. Example geodesics of the cone geometry with $\nu = 0.3$ (corresponding to a deficit angle $\approx 0.24\pi$) from Eq. (62). These satisfy $r_0 = 2, \theta_0 = \pi/2$, and varying ϕ_0 . As the geodesics approach the origin, they become the union of two rays.

the geodesics are

$$\begin{aligned} r(t) &= \pm \sqrt{(r_0 + t \cos \vartheta_0)^2 + (1 - \nu)t^2 \sin^2(2\vartheta_0)/4} \\ \theta(t) - \theta_0 &= \frac{1}{\sqrt{1 - \nu}} (\tan^{-1}(\gamma t + \delta) - \tan^{-1} \delta) \end{aligned} \quad (62)$$

where

$$\begin{aligned} \gamma &= -\frac{\cot(\vartheta_0)}{2\sqrt{1 - \nu}r_0} ((1 - \nu) \cos(2\vartheta_0) + \nu - 3) \\ \delta &= \frac{\csc \vartheta_0}{\sqrt{1 - \nu}}. \end{aligned} \quad (63)$$

Example geodesics are plotted in Fig. 4 for $\nu = 0.3$.

Geodesics from trivial coordinates

Alternatively, we can solve the geodesic equation for the radial spiral spin texture by taking coordinates in which the metric is trivial. To find such coordinates, we start with the effective line element for the radial spiral:

$$dl^2 = dx^2 + dy^2 + dz_{\text{eff}}^2, \quad (64)$$

where z_{eff} is the embedding coordinate. For the radial spiral, $z_{\text{eff}} = \frac{\pi l_C}{\lambda_s} r$ where $r = \sqrt{x^2 + y^2}$. Therefore, in the polar coordinates (r, θ) with $r \geq 0, 0 \leq \theta < 2\pi$, the line element is given by

$$dl^2 = \left(\frac{dr}{1 - \alpha} \right)^2 + r^2 d\theta^2, \quad (65)$$

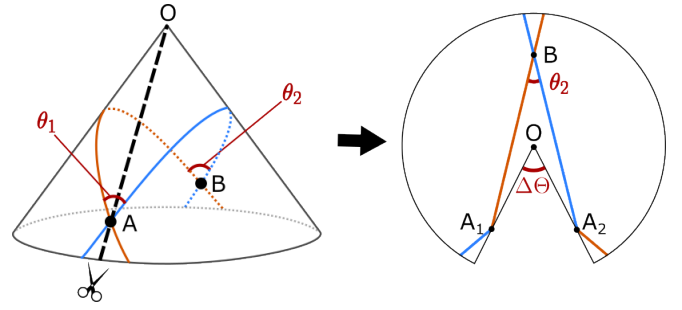


FIG. 5. Geodesics on a cone and the corresponding net. The left panel shows geodesics on the cone intersecting at points A and B, with interior angles θ_1 and θ_2 . The right panel shows the net obtained by cutting the cone along line OA, where points A_1 and A_2 both represent the same point A on the cone. The angle $\Delta\Theta$ denotes the cone's angle deficit.

where $\alpha = 1 - 1/\sqrt{1 + (\pi l_C/\lambda_s)^2}$. Then we can see that the metric is trivial in a coordinate $(R, \Theta) = (r/(1 - \alpha), (1 - \alpha)\theta)$. In this new coordinate, the line element becomes

$$dl^2 = dR^2 + R^2 d\Theta = dX^2 + dY^2, \quad (66)$$

where $X = R \cos \Theta, Y = R \sin \Theta$. Therefore, in these new coordinates (R, Θ) or (X, Y) , the metric is that of a flat space. Note that Θ now only takes values between $0 \leq \Theta < 2\pi(1 - \alpha)$ with angle deficit $\Delta\Theta \equiv 2\pi\alpha$. Intuitively, the effective curved space of a radial spiral is equivalent to a cone, and (X, Y) is the coordinate on the cone's net. Correspondingly, the deficit of Θ from 2π , $\Delta\Theta$, is the angle deficit of the cone (also see Fig. 5).

Since the metric in (X, Y) coordinates is trivial, the trajectory of a particle is a straight line with constant velocity in (X, Y) coordinates: $\mathbf{X}(t) = \mathbf{X}_0 + \mathbf{V}t$. Such straight lines can be expressed with R, Θ as

$$R \cos(\Theta - \Theta_0) = \text{const.} \quad (67)$$

with a constant Θ_0 . Rewriting this with r, θ coordinates, we find

$$r \cos((1 - \alpha)(\theta - \theta_0)) = \text{const.} \quad (68)$$

When a particle comes from $r = \infty$ at $t = -\infty$, passes by around the origin and goes to $r = \infty$ at $t = +\infty$, θ at $t = \pm\infty$ has to satisfy either $(1 - \alpha)(\theta - \theta_0) = \pm\pi/2$. Therefore, θ at $t = \pm\infty$ is either $\theta_{\pm} = \pm\frac{\pi}{2(1 - \alpha)} + \theta_0$. In particular, the deflection angle φ is given by:

$$|\varphi| = \pi - (\theta_+ - \theta_-) = \frac{\pi\alpha}{1 - \alpha}. \quad (69)$$

This deflection angle is clearly seen in Fig. 4.

We can also confirm the relation between the interior angles θ_1, θ_2 and the Gauss curvature K in the main text, $\theta_1 + \theta_2 = K$, for the radial spiral by considering the geodesics on the cone's net. Consider when two geodesics

intersect at two points A and B with interior angles θ_1 and θ_2 , as illustrated in the left panel of Fig. 5. We can obtain the corresponding net by cutting the cone along line OA, which is shown in the right panel. Noting that the sum of the interior angles of a polygon OA_2BA_1 is 2π and that $\angle OA_1B + \angle OA_2B = \theta_1$, we find $\Delta\Theta = \theta_1 + \theta_2$. Since the integrated Gaussian curvature K enclosed by the two geodesics is nothing but the angle deficit $\Delta\Theta$, we confirm $\theta_1 + \theta_2 = K$. We also note that the relation between the deflection angle φ and the Gauss curvature K in the main text, $\varphi = K$, does not apply to the current case, because the curved metric in the radial spiral is not localized as we assumed in deriving the relation.

While the deflection of geodesics in a curved space is qualitatively different than scattering off of a potential, we may note the following: deflection of geodesics in the cone geometry, and indeed any geometry with positive Gaussian curvature, resembles scattering due to a potential well, while deflection due to a negative curvature would resemble scattering off of a potential barrier. This follows from the Gauss-Bonnet theorem: when curvature is positive, a pair of geodesics can close to form a polygon, while when the curvature is negative this is not possible. When electrons scatter due to a localized spin texture (outside of which spins are uniform), the potential V always acts as a barrier, while the emergent metric may scatter electrons in a manner resembling either a potential barrier or well (with Fig. 4 depicting the latter).

Other properties of the radial spiral spin texture

Let us discuss two properties of the radial spiral spin texture: (1) uniqueness properties and (2) approximation of realistic spin textures obtained from minimizing spin gradient energy.

Uniqueness. The radial spiral is the unique spin spiral which is coplanar, continuous, rotationally symmetric, and has constant squared gradient $\sum_i (\partial_i \mathbf{S})^2$. In fact, this is true for the analog of the radial spiral in higher than two dimensions as well, though here we prove it for $d = 2$. Uniqueness here is implicitly up to a spatially constant rotation in spin space, $\mathbf{S}(\mathbf{x}) \mapsto R\mathbf{S}(\mathbf{x})$ where $R \in SO(3)$.

To prove this, first let us apply a rotation so that $\mathbf{S} \cdot \hat{z} = 0$. Then we can assume

$$\mathbf{S}(\mathbf{x}) = (\cos f(r), \sin f(r), 0) \quad (70)$$

in order to maintain $|\mathbf{S}| = 1$ and rotational symmetry. Then $f''(r) = \text{constant}$, which implies $f(r) = ar + b$, and we may assume $b = 0$ by applying an appropriate rotation.

Minimizing spin gradient energy. In the main text, we mentioned that the radial spiral approximately describes configurations minimizing the spin gradient energy in

geometries with radial boundary conditions $\mathbf{S}(r_{\min}) \neq \mathbf{S}(r_{\max})$. Here, we explain this further.

Consider the problem of finding the normalized spin texture $\mathbf{S}(\mathbf{x})$ which minimizes the spin gradient energy

$$E[\mathbf{S}] = \frac{K}{2} \int_{\Omega} [d\mathbf{x}] (\partial_i \mathbf{S})^2 \quad (71)$$

in a disk Ω with radius r_{\max} subject to the following boundary conditions: $\mathbf{S}(r = r_{\max}) = \mathbf{S}_1$ and $\mathbf{S}(r \leq r_{\min}) = \mathbf{S}_0$ for some $r_{\min} < r_{\max}$. For instance, this could describe a region of a ferromagnet outside of which spins point up, but inside of which spins are forced to point in-plane due to a local Zeeman field.

Minimum energy configurations wind only in the $\mathbf{S}_1, \mathbf{S}_0$ plane. Without loss of generality, we assume $\mathbf{S}_1 = \hat{y}, \mathbf{S}_0 = \hat{x}$, and take (for two dimensions)

$$\mathbf{S}(\mathbf{x}) = (\cos f(r, \theta), \sin f(r, \theta), 0). \quad (72)$$

The energy density is $(\partial_r f)^2 + r^{-2}(\partial_\theta f)^2$. Since θ -dependence only increases energy, we take $f(r, \theta) = f(r)$ and find $E[\mathbf{S}] = \frac{K}{2} \int_{r_{\min}}^{r_{\max}} dr r (\partial_r f)^2$. From the Euler-Lagrange equation $\partial_r(r \partial_r f) = 0$ it follows that $f(r) = a \ln r + b$, and matching boundary conditions yields

$$f(r) = \frac{\pi}{2} \frac{\ln(r/r_{\min})}{\ln(r_{\max}/r_{\min})}. \quad (73)$$

At any radius $r_{\min} < r_* < r_{\max}$, $f(r)$ can of course be locally approximated to linear order as

$$f(r) \approx \frac{\pi}{2} \frac{\ln(r_*/r_{\min})}{\ln(r_{\max}/r_{\min})} + \frac{\pi}{2r_* \ln(r_{\max}/r_{\min})} (r - r_*) \quad (74)$$

and agrees with the radial spiral. The analogous energy minimization problem in d dimensions yields $f(r) \sim r^{2-d}$, and a linear approximation once again is valid locally, agreeing with the radial spiral. In this sense, the radial spiral *locally* describes an energy minimizing configuration with appropriate radial boundary conditions.

Ferromagnet/ spin-helical domain wall

We expand upon the discussion of the transition between ferromagnet and spin-helical regions in the main text. This is a simple setup which captures the bending of geodesics. We take

$$\mathbf{S}(\mathbf{x}) = (0, \sin f(\mathbf{x}), \cos f(\mathbf{x}))$$

$$f(\mathbf{x}) = f(x) = \begin{cases} 0 & x \rightarrow -\infty \\ \frac{2\pi x}{\lambda_s} & x \rightarrow +\infty \end{cases} \quad (75)$$

We plot this in Fig. 6. This sort of texture could arise in a material with a natural tendency to a helical phase (e.g. with the DMI) and a ferromagnet phase (strong Zeeman field) near a first-order transition; or in the helical phase

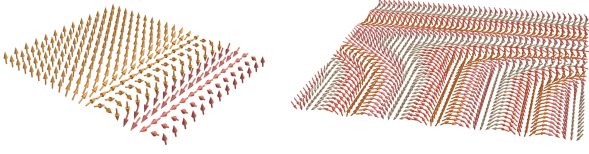


FIG. 6. Left: the spin texture of Eq. (75). Right: the spin texture of Eq. (87).

with an inhomogenous Zeeman field which turns one side of the material into a ferromagnet.

It is straightforward to see that geodesics will bend across the boundary $x = 0$. The metric is

$$g^{ij} = \delta^{ij} - \frac{l_C^2}{4} f'(x)^2 \delta^{ix} \delta^{jx}. \quad (76)$$

Geodesics conserve the energy

$$E = \frac{1}{2} m g_{ij} \dot{x}^i \dot{x}^j. \quad (77)$$

To see this, note that

$$\begin{aligned} \dot{E}/m &= \frac{1}{2} \dot{x}^k \partial_k g_{ij} \dot{x}^i \dot{x}^j + g_{ij} \ddot{x}^i \dot{x}^j \\ &= \frac{1}{2} \dot{x}^k (\Gamma_{ki}^m g_{mj} + \Gamma_{kj}^m g_{mi}) \dot{x}^i \dot{x}^j + g_{ij} \ddot{x}^i \dot{x}^j \\ &= (g_{ij} \ddot{x}^i + \Gamma_{ki}^m g_{mj} \dot{x}^k \dot{x}^i) \dot{x}^j \\ &= \dot{x}^j g_{rj} (\ddot{x}^r + \Gamma_{ki}^r \dot{x}^k \dot{x}^i) \\ &= 0. \end{aligned} \quad (78)$$

Hence

$$E = \frac{1}{2} m \left(1 + \frac{1}{4} l_C^2 f'(x)^2 \right) \dot{x}^2 + \frac{1}{2} m \dot{y}^2 = \text{const.} \quad (79)$$

Because the system has a y translation invariance, $p_y = m g_{yi} \dot{x}^i$ is conserved. Hence $\dot{y} = \text{constant}$ and also

$$\left(1 + \frac{1}{4} l_C^2 f'(x)^2 \right) \dot{x}^2 = \text{const.} \quad (80)$$

Let $v_{L/R}$ denote the x -velocity for $x \rightarrow \mp\infty$. It follows that

$$\left(1 + \frac{\pi^2 l_C^2}{\lambda_s^2} \right) v_R^2 = v_L^2 \quad (81)$$

giving us the relation

$$\frac{v_R}{v_L} = \frac{1}{\sqrt{1 + (\pi l_C / \lambda_s)^2}}. \quad (82)$$

Let $\theta_{L/R}$ be the angle of the geodesic with respect to the x axis in the left and right regions, respectively. It follows that

$$\frac{\tan \theta_R}{\tan \theta_L} = \sqrt{1 + (\pi l_C / \lambda_s)^2}. \quad (83)$$

While this agrees with Snell's law $\sin \theta_L / \sin \theta_R = n_R / n_L$ for light traveling between two isotropic media with indices of refraction $n_{L/R}$ for *small* angles $\theta_{L/R}$, it differs for larger angles. This distinction has the important consequence that there is no condition for total internal reflection for the relation above.

So far, we've been ignoring the effect of $V(\mathbf{x}) = \hbar^2 f'(x)^2 / 2m$. If we include the effect of V , the geodesics instead conserve the energy

$$E = \frac{1}{2} m g_{ij} \dot{x}^i \dot{x}^j + V \quad (84)$$

and following the same steps,

$$\frac{1}{2} (1 + (\pi l_C / \lambda_s)^2) v_R^2 + \frac{h^2}{2m^2 \lambda_s^2} = \frac{1}{2} v_L^2. \quad (85)$$

The resulting relation between asymptotic angles is modified to

$$\frac{v_R}{v_L} = \frac{\tan \theta_L}{\tan \theta_R} = \frac{\sqrt{1 - \frac{h^2}{m^2 \lambda_s^2 v_L^2}}}{\sqrt{1 + \frac{\pi^2 l_C^2}{\lambda_s^2}}}. \quad (86)$$

Hence both V and g^{ij} contribute to the bending of trajectories. We can isolate the effect from g^{ij} by considering a domain wall between two distinct spiral phases, which we turn to next.

Spiral / spiral domain wall

Consider a spin texture which interpolates between two distinct spiral phases with wavevectors $\mathbf{q}_L = q\hat{x}$ and $\mathbf{q}_R = q\hat{y}$ as x goes from $-\infty$ to $+\infty$. This could capture a domain wall in a chiral magnet which has multiple degenerate ground state spiral solutions. Concretely, consider

$$\begin{aligned} \mathcal{S}(\mathbf{x}) &= (0, \sin \mathbf{q}(x) \cdot \mathbf{x}, \cos \mathbf{q}(x) \cdot \mathbf{x}) \\ \mathbf{q}(x) &= \begin{cases} \frac{2\pi}{\lambda_s} \hat{x} & x \rightarrow -\infty \\ \frac{2\pi}{\lambda_s} \hat{y} & x \rightarrow +\infty \end{cases} \end{aligned} \quad (87)$$

as shown, for instance, in Fig. 6. The metric far to the left and far to the right takes the form

$$\begin{aligned} g_L^{ij} &= \delta^{ij} - \frac{\pi^2 l_C^2}{\lambda_s^2} \delta^{ix} \delta^{jx} \\ g_R^{ij} &= \delta^{ij} - \frac{\pi^2 l_C^2}{\lambda_s^2} \delta^{iy} \delta^{jy} \end{aligned} \quad (88)$$

while $V(\mathbf{x}) = \hbar^2 / 2m\lambda_s^2$ in both cases. Therefore we can ignore the effect of $V(\mathbf{x})$ for the asymptotic behavior of geodesics and proceed by studying the conserved energy $E = \frac{1}{2} m g_{ij} \dot{x}^i \dot{x}^j$. In the asymptotic regions, we have

$$\begin{cases} (1 + (\pi l_C / \lambda_s)^2) \dot{x}^2 + \dot{y}^2 = C & x \rightarrow -\infty \\ (1 + (\pi l_C / \lambda_s)^2) \dot{y}^2 + \dot{x}^2 = C & x \rightarrow +\infty \end{cases} \quad (89)$$

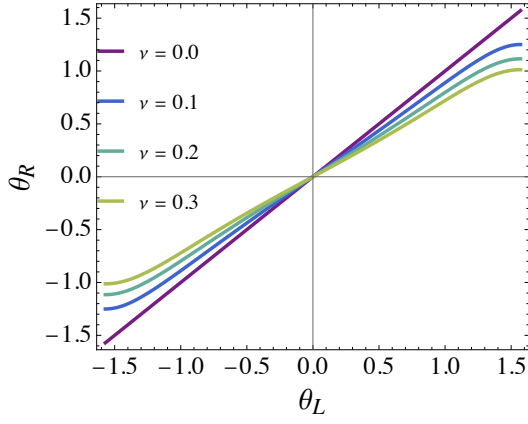


FIG. 7. Plot of Eq. (93) for a geodesic across a spiral / spiral domain wall.

with C a constant. Assuming the metric globally only depends on x , the y momentum $p_y = mg_{yi}\dot{x}^i$ is conserved. In the asymptotic regions, we have

$$\begin{cases} p_y = m\dot{y} & x \rightarrow -\infty \\ p_y = m(1 + (\pi l_C/\lambda_s)^2)\dot{y} & x \rightarrow +\infty. \end{cases} \quad (90)$$

Let us parameterize

$$(\dot{x}, \dot{y}) = \begin{cases} v_L(\cos \theta_L, \sin \theta_L) & x \rightarrow -\infty \\ v_R(\cos \theta_R, \sin \theta_R) & x \rightarrow +\infty \end{cases} \quad (91)$$

in the asymptotic regions, and for convenience let

$$\nu = (\pi l_C/\lambda_s)^2. \quad (92)$$

Solving the system of equations yields

$$\tan \theta_R = \frac{\tan \theta_L}{\sqrt{(1+\nu)^3 + \nu(1+\nu)\tan^2 \theta_L}}. \quad (93)$$

This relation is plotted in Fig. 7. To leading order and at small angles, we have

$$\theta_R - \theta_L \approx -\frac{3}{2}\theta_L \frac{\pi^2 l_C^2}{\lambda_s^2}. \quad (94)$$

Summary of Riemannian geometry

In this section, we summarize the results from Riemannian geometry used in the main text. For a thorough description of the Riemannian geometry, see, for example, Ref. [23, 24].

Basics of Riemannian geometry

Consider d -dimensional Riemannian manifold M . The line element on M defines the metric g_{ij} as

$$dl^2 = g_{ij} dx^i dx^j, \quad (95)$$

where $x^i (i = 1, \dots, d)$ is the (local) coordinate. The metric defines the inner product between vectors A and B , which we denote as $g(A, B) \equiv g_{ij} A^i B^j$. We can define the Levi-Civita connection associated with the metric g_{ij} . The corresponding Christoffel symbol is given by

$$\Gamma_{jk}^i = \frac{g^{im}}{2} (\partial_k g_{mj} + \partial_j g_{mk} - \partial_m g_{jk}), \quad (96)$$

where $\partial_i = \partial/\partial x^i$. With the Christoffel symbol, we can define the covariant derivative of vectors. For a vector A , its covariant derivative in i -direction, $\nabla_i A$, is given by

$$(\nabla_i A)^j = \partial_i A^j + \Gamma_{ik}^j A^k. \quad (97)$$

The Riemann curvature tensor $R^i{}_{jkl}$ is defined as follows. We denote the basis vector in i -direction as e_i . e_i is what is identified with the partial derivative ∂_i in mathematics literature. $R^i{}_{jkl}$ is then defined through the following relation:

$$[\nabla_k, \nabla_l] e_j = R^i{}_{jkl} e_i. \quad (98)$$

We can show $R^i{}_{jkl}$ is written with the Christoffel symbol as

$$R^i{}_{jkl} = \partial_k \Gamma_{lj}^i - \partial_l \Gamma_{kj}^i + \Gamma_{km}^i \Gamma_{lj}^m - \Gamma_{lm}^i \Gamma_{kj}^m. \quad (99)$$

Gauss-Bonnet theorem

Here we assume $d = 2$. Gauss-Bonnet theorem relates a closed loop on a two-dimensional curved surface to the Gaussian curvature enclosed by the loop. Consider a closed loop C , parameterized by its arclength s as $x^i(s)$. C is parametrized so that the vector $\dot{x} \equiv dx/ds$ rotates in counterclockwise. C can have vertices with an exterior angle ϕ_i . Then the Gauss-Bonnet theorem states that the following relation holds for a closed loop C :

$$\int_C k_g ds + \int_S \kappa \sqrt{\det g_{ij}} d^2x + \sum_i \phi_i = 2\pi \chi(S). \quad (100)$$

Here, S is the region enclosed by C and $\chi(S)$ is the Euler characteristic. κ is the Gaussian curvature, given by

$$\kappa = \frac{R_{xyxy}}{\det g_{ij}}, \quad (101)$$

where $R_{ijkl} = g_{im} R^m{}_{jkl}$. k_g is the geodesic curvature of the curve C , defined as

$$k_g = g(\nabla_s \dot{x}, a). \quad (102)$$

Here, $\dot{x} = dx/ds$ is the tangent vector along the curve C . Since s is the arclength, \dot{x} is a unit vector: $g(\dot{x}, \dot{x}) = 1$. a is a unit vector orthogonal to \dot{x} , satisfying $g(\dot{x}, a) = 0$, $g(a, a) = 1$. As we consider a two-dimensional surface, a is unique up to sign, and we fix the sign so that (\dot{x}, a)

forms a local right-handed basis. $(\nabla_s \hat{x})^i = \ddot{x}^i + \Gamma_{jk}^i \dot{x}^j \dot{x}^k$ is the covariant derivative of \hat{x} along the curve, with $\ddot{x}^i = d^2 x^i / ds^2$. Since $\nabla_s \hat{x}$ vanishes when C is a geodesic, k_g also vanishes for a geodesic. Therefore, k_g measures the deviation of the curve from geodesics.

When C is a polygon made of geodesics, $\chi(S) = 1$ and $k_g = 0$. Therefore, it follows

$$\int_S \kappa \sqrt{\det g_{ij}} d^2 x + \sum_i \phi_i = 2\pi. \quad (103)$$

This is what we used in the main text.

Relation to the quantum geometry

In this section, we briefly comment on the relation between the emergent curved space and the quantum geometry.

As discussed in the main text, the emergent curved space is characterized by the effective metric given by $g_{ij} = \delta_{ij} + l_C^2 G_{ij}$, with G_{ij} the quantum metric. On the other hand, the quantum metric G_{ij} defines the Riemannian geometry of the Hilbert space, which we here call *quantum Riemannian geometry*. In the same way as the standard Riemannian geometry, we can define the Christoffel symbol and the Riemann curvature as:

$$\gamma_{jk}^i = \frac{(G^{-1})^{im}}{2} (\partial_k G_{mj} + \partial_j G_{mk} - \partial_m G_{jk}), \quad (104)$$

$$r_{jkl}^i = \partial_k \gamma_{jl}^i - \partial_l \gamma_{kj}^i + \gamma_{km}^i \gamma_{lj}^m - \gamma_{lm}^i \gamma_{kj}^m. \quad (105)$$

r_{jkl}^i represents the curvature of the Hilbert space, and we may call the quantum Riemann curvature tensor. We assume here that G_{ij} is positive definite so that we can define its inverse G^{-1} .

In this case, the Riemann curvature of the emergent space, R_{ijkl} , is directly related to the quantum Riemann curvature, r_{ijkl} :

$$R_{ijkl}^i = l_C^2 r_{ijkl}^i. \quad (106)$$

* yugo0o24@mit.edu

† npaul@mit.edu

- [1] G. Sundaram and Q. Niu, Wave-packet dynamics in slowly perturbed crystals: Gradient corrections and Berry-phase effects, *Physical Review B* **59**, 14915 (1999), publisher: American Physical Society.
- [2] G. E. Volovik, Linear momentum in ferromagnets, *Journal of Physics C: Solid State Physics* **20**, L83 (1987).
- [3] D. Loss, P. Goldbart, and A. V. Balatsky, Berry's phase and persistent charge and spin currents in textured mesoscopic rings, *Physical Review Letters* **65**, 1655 (1990).

- [4] J. Ye, Y. B. Kim, A. J. Millis, B. I. Shraiman, P. Majumdar, and Z. Tešanović, Berry Phase Theory of the Anomalous Hall Effect: Application to Colossal Magnetoresistance Manganites, *Physical Review Letters* **83**, 3737 (1999).
- [5] Y. Taguchi, Y. Oohara, H. Yoshizawa, N. Nagaosa, and Y. Tokura, Spin Chirality, Berry Phase, and Anomalous Hall Effect in a Frustrated Ferromagnet, *Science* **291**, 2573 (2001).
- [6] M. Onoda, G. Tatara, and N. Nagaosa, Anomalous Hall Effect and Skyrmion Number in Real and Momentum Spaces, *Journal of the Physical Society of Japan* **73**, 2624 (2004).
- [7] A. Neubauer, C. Pfeleiderer, B. Binz, A. Rosch, R. Ritz, P. G. Niklowitz, and P. Böni, Topological Hall Effect in the $\$A\$$ Phase of MnSi, *Physical Review Letters* **102**, 186602 (2009), publisher: American Physical Society.
- [8] K. Ohgushi, S. Murakami, and N. Nagaosa, Spin anisotropy and quantum Hall effect in the kagome lattice: Chiral spin state based on a ferromagnet, *Physical Review B* **62**, R6065 (2000), publisher: American Physical Society.
- [9] P. Bruno, V. K. Dugaev, and M. Taillefer, Topological Hall Effect and Berry Phase in Magnetic Nanostructures, *Physical Review Letters* **93**, 096806 (2004), publisher: American Physical Society.
- [10] K. Hamamoto, M. Ezawa, and N. Nagaosa, Quantized topological Hall effect in skyrmion crystal, *Physical Review B* **92**, 115417 (2015), publisher: American Physical Society.
- [11] Z. Addison, L. Keyes, and M. Randeria, Anomalous and Topological Hall Effects with Phase-Space Berry Curvatures: Electric, Thermal, and Thermoelectric Transport in Magnets (2024), arXiv:2409.04376 [cond-mat].
- [12] T. Park, X. Huang, L. Savary, and L. Balents, Quantum geometry from the Moyal product: quantum kinetic equation and non-linear response (2025), arXiv:2504.10447 [cond-mat].
- [13] N. Paul, Y. Zhang, and L. Fu, Giant proximity exchange and flat Chern band in 2D magnet-semiconductor heterostructures, *Science Advances* **9**, eabn1401 (2023), publisher: American Association for the Advancement of Science.
- [14] P. Schneider, J. Ehlers, and E. E. Falco, *Gravitational Lenses*, edited by I. Appenzeller, G. Börner, M. Harwit, R. Kippenhahn, J. Lequeux, P. A. Strittmatter, and V. Trimble, *Astronomy and Astrophysics Library* (Springer Berlin Heidelberg, Berlin, Heidelberg, 1992).
- [15] T. Fujita, M. B. A. Jalil, S. G. Tan, and S. Murakami, Gauge fields in spintronics, *Journal of Applied Physics* **110**, 121301 (2011).
- [16] S. G. Tan, S.-H. Chen, C. S. Ho, C.-C. Huang, M. B. A. Jalil, C. R. Chang, and S. Murakami, Yang-Mills physics in spintronics, *Physics Reports Yang-Mills physics in spintronics*, **882**, 1 (2020).
- [17] P. G. De Gennes, Effects of Double Exchange in Magnetic Crystals, *Physical Review* **118**, 141 (1960).
- [18] T. Ohnishi and N. Nagaosa, Adiabatic Approximation for Path Integrals and Geometrical Potentials, *Journal of the Physical Society of Japan* **76**, 015003 (2007), publisher: The Physical Society of Japan.
- [19] Y. Aharonov, Origin of the geometric forces accompanying Berry's geometric potentials, *Physical Review Letters*

- 69**, 3593 (1992).
- [20] M. V. Berry and J. M. Robbins, Classical geometric forces of reaction: an exactly solvable model, Proceedings of the Royal Society of London. Series A: Mathematical and Physical Sciences **442**, 641 (1997), publisher: Royal Society.
- [21] We note that the Hamiltonian for a particle in curved space can commonly take a different form, but we can show that the two formulations are equivalent up to $\mathcal{O}(l_C^2 \lambda_s^{-4})$. See SM for more details.
- [22] S. Deser, R. Jackiw, and G. 't Hooft, Three-dimensional Einstein gravity: Dynamics of flat space, Ann. Phys. **152**, 220 (1984).
- [23] M. Nakahara, Geometry, Topology and Physics, 2nd ed. (CRC Press, Boca Raton, 2018).
- [24] S. Kobayashi, Differential Geometry of Curves and Surfaces, Springer Undergraduate Mathematics Series (Springer Singapore, Singapore, 2019).
- [25] After completing this work, we found similar relations for the true gravitational lensing of light in Ref. [52].
- [26] R. Egerton, Physical Principles of Electron Microscopy (Springer International Publishing, Cham, 2016).
- [27] J. E. Avron, R. Seiler, and P. G. Zograf, Viscosity of Quantum Hall Fluids, Physical Review Letters **75**, 697 (1995).
- [28] T. L. Hughes, R. G. Leigh, and E. Fradkin, Torsional Response and Dissipationless Viscosity in Topological Insulators, Physical Review Letters **107**, 075502 (2011), publisher: American Physical Society.
- [29] B. Bradlyn, M. Goldstein, and N. Read, Kubo formulas for viscosity: Hall viscosity, Ward identities, and the relation with conductivity, Physical Review B **86**, 245309 (2012).
- [30] L. Dong and Q. Niu, Geometrodynamics of electrons in a crystal under position and time-dependent deformation, Physical Review B **98**, 115162 (2018), publisher: American Physical Society.
- [31] P. Rao and B. Bradlyn, Hall Viscosity in Quantum Systems with Discrete Symmetry: Point Group and Lattice Anisotropy, Physical Review X **10**, 021005 (2020).
- [32] J. P. Dahlhaus, C.-Y. Hou, A. R. Akhmerov, and C. W. J. Beenakker, Geodesic scattering by surface deformations of a topological insulator, Physical Review B **82**, 085312 (2010).
- [33] U. R. Fischer and M. Visser, Riemannian Geometry of Irrotational Vortex Acoustics, Physical Review Letters **88**, 110201 (2002), publisher: American Physical Society.
- [34] G. E. Volovik, Black hole and Hawking radiation by type-II Weyl fermions, JETP Letters **104**, 645 (2016), company: Springer Distributor: Springer Institution: Springer Label: Springer Number: 9 Publisher: Pleiades Publishing.
- [35] A. Westström and T. Ojanen, Designer Curved-Space Geometry for Relativistic Fermions in Weyl Metamaterials, Physical Review X **7**, 041026 (2017).
- [36] L. Liang and T. Ojanen, Curved spacetime theory of inhomogeneous Weyl materials, Physical Review Research **1**, 032006 (2019), publisher: American Physical Society.
- [37] H. Huang, K.-H. Jin, and F. Liu, Black-hole horizon in the Dirac semimetal Zn 2 In 2 S 5, Physical Review B **98**, 121110 (2018).
- [38] M. A. Zubkov, The black hole interior and the type II Weyl fermions, Modern Physics Letters A **33**, 1850047 (2018), publisher: World Scientific Publishing Co.
- [39] M. A. Zubkov, Emergent gravity and chiral anomaly in Dirac semimetals in the presence of dislocations, Annals of Physics **360**, 655 (2015).
- [40] S. Guan, Z.-M. Yu, Y. Liu, G.-B. Liu, L. Dong, Y. Lu, Y. Yao, and S. A. Yang, Artificial gravity field, astrophysical analogues, and topological phase transitions in strained topological semimetals, npj Quantum Materials **2**, 23 (2017), publisher: Nature Publishing Group.
- [41] J. Nissinen and G. E. Volovik, Type-III and IV interacting Weyl points, JETP Letters **105**, 447 (2017).
- [42] V. Könye, L. Mertens, C. Morice, D. Chernyavsky, A. G. Moghaddam, J. van Wezel, and J. van den Brink, Anisotropic optics and gravitational lensing of tilted Weyl fermions, Physical Review B **107**, L201406 (2023), publisher: American Physical Society.
- [43] A. Haller, S. Hegde, C. Xu, C. De Beule, T. L. Schmidt, and T. Meng, Black hole mirages: Electron lensing and Berry curvature effects in inhomogeneously tilted Weyl semimetals, SciPost Physics **14**, 119 (2023).
- [44] S. E. Barnes and S. Maekawa, Generalization of Faraday's Law to Include Nonconservative Spin Forces, Physical Review Letters **98**, 246601 (2007).
- [45] N. Nagaosa and Y. Tokura, Topological properties and dynamics of magnetic skyrmions, Nature Nanotechnology **8**, 899 (2013), publisher: Nature Publishing Group.
- [46] S. A. Yang, G. S. D. Beach, C. Knutson, D. Xiao, Q. Niu, M. Tsoi, and J. L. Erskine, Universal Electromotive Force Induced by Domain Wall Motion, Physical Review Letters **102**, 067201 (2009).
- [47] Y. Yamane, K. Sasage, T. An, K. Harii, J. Ohe, J. Ieda, S. E. Barnes, E. Saitoh, and S. Maekawa, Continuous Generation of Spinmotive Force in a Patterned Ferromagnetic Film, Physical Review Letters **107**, 236602 (2011), publisher: American Physical Society.
- [48] Y. Yamane, J. Ieda, and J. Sinova, Electric voltage generation by antiferromagnetic dynamics, Physical Review B **93**, 180408 (2016).
- [49] L. Chojnacki, R. Pohle, H. Yan, Y. Akagi, and N. Shannon, Gravitational wave analogs in spin nematics and cold atoms, Physical Review B **109**, L220407 (2024), publisher: American Physical Society.
- [50] X. G. Wen and A. Zee, Shift and spin vector: New topological quantum numbers for the Hall fluids, Physical Review Letters **69**, 953 (1992).
- [51] B. Estienne, N. Regnault, and V. Crépel, Ideal Chern bands as Landau levels in curved space, Physical Review Research **5**, L032048 (2023).
- [52] G. W. Gibbons and M. C. Werner, Applications of the Gauss–Bonnet theorem to gravitational lensing, Classical and Quantum Gravity **25**, 235009 (2008).